Received: 14 July 2020 | Revised: 20 August 2020 | Accepted: 15 September 2020

DOI: 10.1002/pen.25546

RESEARCH ARTICLE

POLYMER ENGINEERING AND SCIENCE WILEY

Re-entrant auxetic structures fabricated by fused deposition modeling: An experimental study of influence of process parameters under compressive loading

Swapnil Vyavahare | **Shailendra Kumar**

Mechanical Engineering Department, Sardar Vallabhbhai National Institute of Technology, Surat, Gujarat, India

Correspondence
Shailendra Kumar, Mechanical Engineering Department, Sardar Vallabhbhai National Institute of Technology, Surat, Gujarat, India.
Email: skbudhwar@med.svnit.ac.in

Abstract

The present article is focused on investigating the influence of process parameters under compressive loading in case of reentrant auxetic structures fabricated by fused deposition modeling (FDM). Auxetic structures of acrylonitrile butadiene styrene (ABS) and poly-lactic acid (PLA) materials are fabricated. Three process parameters of FDM namely layer thickness, raster angle, and number of contours are considered to investigate their influence on compressive strength, stiffness, and specific energy absorption (SEA). Experiments are performed on the basis of central composite design and analysis is performed using ANOVA. It is found that compressive strength of auxetic structure improves with increase in layer thickness. But with increase in raster angle, it increases first and then decreases. Compressive stiffness of structures initially decreases and then increases with increase in raster angle, while it increases with increase in number of contours. SEA of structures increases with decrease in layer thickness. Based on the analysis of experimental results, regression models are developed to predict these responses. Also, multi-response optimization is performed to optimize strength, stiffness, and SEA. Auxetic structures failed under compressive loading are also examined using scanning electron microscope.

KEYWORDS

compressive strength, fused deposition modeling, layer thickness, number of contours, raster angle, re-entrant auxetic structure, specific energy absorption, stiffness

1 | INTRODUCTION

Auxetic structure is a class of meta-material in which longitudinal compression results in lateral compression. It has negative Poisson's ratio (NPR).[1] The unusual behavior of auxetic structure is due to the geometry of its unit cell; which results in greater in-plane indention resistance, impact resistance, fracture toughness, bending stiffness, and transverse shear modulus as compared to conventional positive Poisson's ratio structures.[2,3] Auxetic structures have wide applications in automotive, aerospace, sports, and marine applications.[4-6] In applications, such as automobile frame, good compressive strength, and stiffness of auxetic structures, is required. While, high specific energy absorption (SEA) is needed in applications, such as vehicle bumper and structure used behind the instrument panel of vehicles. Reentrant type auxetic structures have better mechanical properties than other NPR structures.[2] Strength, stiffness, and SEA of the structure mainly depend on material and fabrication

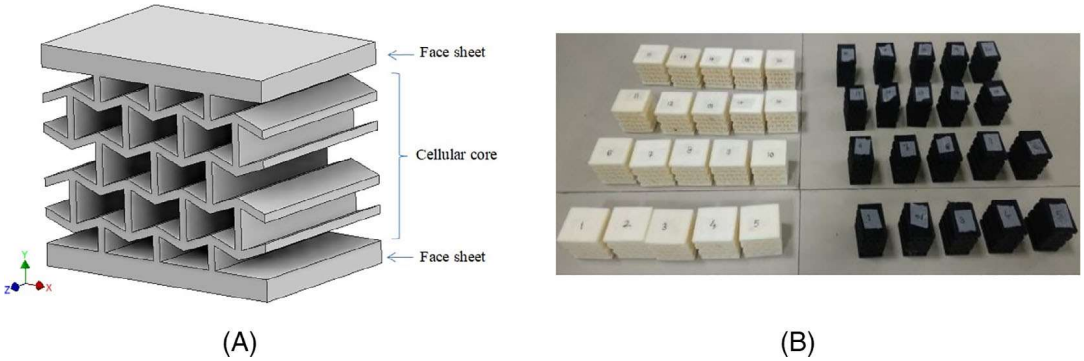

FIGURE 1 A, CAD model of auxetic structure and B, FDM fabricated auxetic structures. CAD, computer-aided design; FDM, fused deposition modeling [Color figure can be viewed at wileyonlinelibrary.com]

TABLE 1 Range of process parameters

Sr. no.	Process parameters	Range
1.	Layer thickness (mm)	0.18-0.38
2.	Raster angle (degree)	0-90
3.	Number of contours	1-3

process.[7-13] Fused deposition modelling (FDM), one technique of additive manufacturing, is capable to fabricate lightweight auxetic structures of various polymers economically.[14-18] Layer thickness, raster angle (direction of raster deposition), and number of contours are some of the major process parameters of FDM influencing responses namely strength, stiffness, and SEA of structures.[19-25] Realistic applications of FDM-fabricated components as load-bearing or energy absorbing structures are very restricted because of their anisotropy.

Several studies have been reported on investigating the influence of process parameters of FDM on mechanical properties of standard fabricated parts.[23-28] A summary of such research efforts is reported in the literature.[29-31] Some efforts have also been made to investigate various structures.[20-25] Because of the heat generated by FDM extruder, the hot layer is bonded by fusion to the previously deposited layer.[19] Ang et al.[20] studied the impact of process parameters on compressive strength and stiffness of tissue engineering scaffold fabricated by FDM. They found that Air gap and raster width are most significant parameters. Dong et al.[21] reported that fan speed and layer thickness are most significant process parameter for inclined and horizontal strut, respectively. Further, they optimized process parameters for improving effective elastic modulus and ultimate compressive strength of lattice structures. Dave et al.[22] found that infill density is most significant process parameter for compressive strength of tissue engineering scaffold. Magalhães et al.[23] observed that stiffness of specimen having sandwich deposition configuration (with raster angle $\pm 45^0$) is higher than the specimen with default configuration (i.e. with zero raster angle). Too et al.[32] investigated the effect of factors on the porosity and compressive strength of the porous structures. A model was established for the forecast of the effect of the air gap on the porosity of the structure. Vanaei et al.[33] concluded that influence of extruder temperature was more on cooling rate of material than other process parameters, such as support temperature, speed, and layer height. Also, investigators focused on significant parameters to optimize the process and ultimately get the combination of factors.[34]

The above literature review reveals that although efforts have been made to study influence of FDM process parameters on mechanical properties of standard components, but no researcher have studied mechanical properties, such as strength, stiffness, and SEA of auxetic structures.[35] Also, there is need to study failure mode of auxetic structures under compressive loading. Therefore, the present work is focused on investigating compressive strength, stiffness, and SEA of reentrant auxetic structures of acrylonitrile butadiene styrene (ABS) and polylactic acid (PLA) fabricated by FDM. Objectives of the present experimental study are following—(a) to study the influence of process parameters on strength, stiffness, and SEA of reentrant auxetic structures under compressive loading; (b) to develop regression models for strength, stiffness, and SEA; (c) to optimize significant process parameters for maximization strength, stiffness, and SEA; and (d) to study failure mode of reentrant auxetic structures.

2 | EXPERIMENTAL

The methodology of present experimental study consists of computer-aided design (CAD) of auxetic structure,

TABLE 2 Design of experiments and results of compressive test of auxetic structures

Design of experiments				ABS material			PLA material		
Run no.	Layer thickness	Raster angle	Number of contour	Compressive strength	Compressive stiffness	SEA	Compressive strength	Compressive stiffness	SEA
	mm	degree		MPa	MPa	J/g	MPa	MPa	J/g
1	0.28	45	2	3.13	53.04	682.43	2.521	62.21	230.42
2	0.28	90	2	3.154	110.54	760.85	2.089	120.11	380.74
3	0.28	45	2	3.3	54.048	663.07	2.623	60.99	218.49
4	0.38	90	3	3.2	134.73	723.48	2.23	148.1	396.78
5	0.28	0	2	2.79	64.78	773.56	1.721	78.89	432.78
6	0.28	45	2	3.202	54.72	659.86	2.419	63.44	215.74
7	0.28	45	3	3.207	66.84	670.42	2.512	75.84	226.48
8	0.38	90	1	2.6	60.74	671.56	2.66	68.42	266.98
9	0.28	45	2	3.21	54.12	669.75	2.427	61.6	243.16
10	0.18	0	1	1.535	54.25	801.29	1.348	62.13	440.74
11	0.18	45	2	3.064	54.13	654.82	2.507	65.74	220.02
12	0.18	90	3	3.014	123.47	745.87	1.873	133.07	372.49
13	0.28	45	2	3.393	54.73	688.85	2.614	62.82	242.74
14	0.18	0	3	2.771	62.74	735.25	1.874	72.84	365.41
15	0.28	45	1	2.302	36.74	670.86	2.447	38.84	229.46
16	0.38	45	2	3.4	58.71	598.78	3.07	68.13	192.74
17	0.18	90	1	1.895	110.74	746.58	1.895	124.71	490.47
18	0.38	0	3	2.952	118.74	727.83	2.258	128.37	465.78
19	0.38	0	1	2.144	51.27	714.89	2.047	59.15	305.42
20	0.28	45	2	3.3	55.89	674.58	2.523	65.69	249.85

Abbreviations: ABS, acrylonitrile butadiene styrene; PLA, poly-lactic acid; SEA, specific energy absorption.

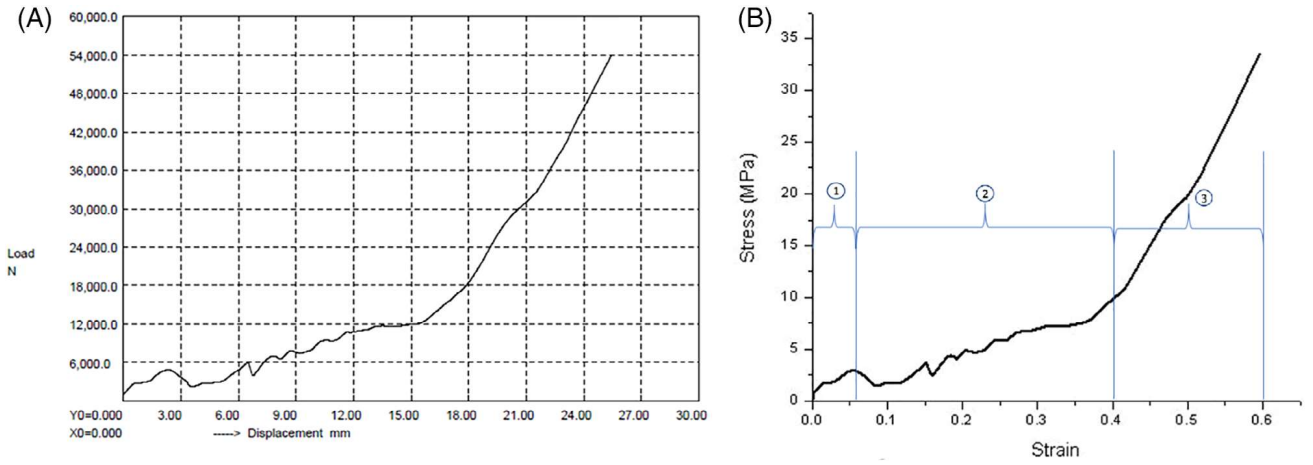

FIGURE 2 A, Load–displacement curve and B, Stress–strain curve for Run no. 1, ABS structure (Region 1-Elastic, Region 2-Plateau, Region 3-Densification). ABS, acrylonitrile butadiene styrene [Color figure can be viewed at wileyonlinelibrary.com]

design of experiment, fabrication, and response measurement. Each step of this methodology is briefly described as under.

2.1 | CAD of auxetic structure

The unit cells of auxetic structure are modeled in the Autodesk Inventor 2020 software and then arranged in the plane and extruded along Z-direction as shown in Figure 1A. To prevent buckling in compressive loading, width of structure is kept as 40 mm.[36] Based on the trial experiments, geometrical parameters (i.e. reentrant angle, arm-length, and height) of unit cell of configurations of auxetic structure are decided. Geometric files of CAD model are saved in stereolithography (STL) format to provide input to the slicer software.

2.2 | Design of experiment

Three control factors of FDM viz. layer thickness, raster angle, and number of contours are taken in the present investigation. Settings of these factors (Table 1) are decided based on the existing experimental set-up. Central composite design technique is used to plan experiments by using the Design- Expert 11 software. As given in Table 2, experimental design suggested total 20 experiments for each material (i.e. ABS and PLA).

2.3 | Fabrication of structures

STL files of auxetic structures are fed to the slicing software; in which levels of control factors are set. GCODE files generated from this software are given to FDM machine (Delta Wasp 2040) for fabrication of structures.[37] Structures are manufactured along Z-direction to avoid use of supports and impact of build orientation on mechanical properties. Also, Z-axis as build orientation and Y-axis as loading direction produces parts with maximum strength as load is carried axially along fibers.[26] For fabrication of ABS structures, print temperature and bed temperature is kept as 240°C and 100°C, respectively. While, for PLA structures, these values are set as 210°C and 60°C, respectively. Infill percentage is kept as 100% for all structures. Inner and outer wall speeds are 60 and 30 mm/s, respectively.

Quasi-two dimensional specimens are fabricated with same number of unit cells (3 × 3). The size of ABS structure and PLA structure is $38 \times 40 \times 66\ mm^3$ and $31 \times 40 \times 48\ mm^3$, respectively. Total 40 structures are fabricated as shown in Figure 1B (PLA structures are shown in black color while ABS structures are shown in white color).

2.4 | Response measurement

Quasi-static uniaxial compressive tests are performed on universal testing machine limited to 60% strain at a cross-head speed of 5 mm/min. Load-displacement curves,

TABLE 3 Means and SD of responses with respect to process parameters

	Material	ABS						PLA					
		Compressive strength (MPa)		Compressive stiffness (MPa)		SEA (J/g)		Compressive strength (MPa)		Compressive stiffness (MPa)		SEA (J/g)	
Process parameter	Levels	Mean	SD	Mean	SD	Mean	SD	Mean	SD	Mean	SD	Mean	SD
Layer thickness (mm)	0.18	2.45	0.7	81.07	33.39	736.76	52.58	1.9	0.41	91.7	34.3	377.83	102.14
	0.28	3.09	0.32	60.54	19.30	691.42	40.92	2.39	0.28	69.042	20.85	266.99	75.46
	0.38	2.85	0.5	84.84	38.82	687.31	54.31	2.45	0.41	94.43	40.76	325.54	107.49
Raster angle (degree)	0	2.43	0.6	70.36	27.63	750.56[a]	35.8	1.85	0.35	80.28	28.04	402.03[a]	65.54
	45	3.15	0.32	54.3	7.37	663.34	24.82	2.57[a]	0.19	62.53	9.39	226.91	16.57
	90	2.77	0.55	108.04[a]	28.29	729.67	35.13	2.15	0.32	118.88[a]	30.15	381.49	79.54
Number of contours	1	2.1	0.36	62.75	25.25	721.04	49.19	2.08	0.51	70.65	32.19	346.61	113.27
	2	3.19[a]	0.17	61.47	16.68	682.66	48.33	2.45	0.35	70.96	18.04	262.67	78.69
	3	3.03	0.16	101.30	30.29	720.57	26.2	2.15	0.28	111.64	34.84	365.39	87.19
	Total	2.88	0.53	71.75	29.37	701.73	49.29	2.28	0.4	81.05	30.92	309.33	97.84

Abbreviations: ABS, acrylonitrile butadiene styrene; PLA, poly-lactic acid; SEA, specific energy absorption.
[a]Maximum average value for every response for all settings of all factors.

TABLE 4 ANOVA results: Main, interaction, and quadratic influence of process parameters on responses

	ABS						PLA					
	Compressive strength (MPa)		Compressive stiffness (MPa)		SEA (J/g)		Compressive strength (MPa)		Compressive stiffness (MPa)		SEA (J/g)	
Process parameter/interaction/quadratic term	F value	*P*	F value	*P*	F value	*P*	F value	*P*	F value	*P*	F value	*P*
Layer thickness (mm)	74.10	<.05	4.42	.06	69.73	<.05	148.87	<.05	5.82	<.05	28.43	<.05
Raster angle (degree)	50.85	<.05	643.60	<.05	12.45	<.05	43.66	<.05	1158.61	<.05	4.39	.06
Number of contours	396.86	<.05	728.68	<.05	0.006	.94	2.38	.16	1306.34	<.05	3.67	.08
Layer thickness and raster angle	0.23	.64	195.31	<.05	0.012	.89	0.04	.85	342.09	<.05	14.03	<.05
Layer thickness and number of contours	20.42	<.05	320.01	<.05	24.69	<.05	12.70	<.05	655.08	<.05	121.56	<.05
Raster angle and number of contours	2.40	.16	0.09	.76	15.51	<.05	34.33	<.05	2.56	.14	2.79	.13
Layer thickness^2	0.0001	.99	5.83	<.05	52.41	<.05	27.83	<.05	18.51	<.05	5.56	<.05
Raster angle^2	33.72	<.05	656.22	<.05	310.67	<.05	229.42	<.05	1184.79	<.05	363.92	<.05
Number of contours^2	113.94	<.05	7.34	<.05	0.27	.61	3.49	.09	20.85	<.05	0.002	.96

Abbreviations: ABS, acrylonitrile butadiene styrene; PLA, poly-lactic acid; SEA, specific energy absorption.

stiffness, and energy absorbed by structures are assessed. Tests are conducted according to ASTM C365 which is a standard test method for flatwise compression properties of sandwich cores.[9,38] Compressive load is applied on the structures along Y-axis (i.e. perpendicular to the build direction) because the bonding strength between each layer of the structure can be tested while loading in Y-direction.[30] Load-displacement curve obtained for auxetic structure (Run no. 1) of ABS material is shown in Figure 2A. Similar curves are obtained in uniaxial compression tests of all auxetic structures, which are further converted in stress-strain curves by measuring dimensions of the specimens. Figure 2B shows a stress-strain curve of auxetic structure (Run no. 1) of ABS material. This curve has three regions (elastic, plateau, and densification). Mechanical properties of structures depend on area under these regions. Bonding between adjacent rasters as well as adjacent layers of the structure is influenced by values of process parameters. Compressive strength, stiffness, and SEA are calculated form stress–strain curves. Compressive strength is determined at yield point obtained before 10% strain. In absence of such yield point, stress at 10% is considered as compressive strength of the structure.[39] Compressive stiffness (i.e. modulus of compression) is calculated by the ratio of stress to strain in elastic region. The total energy absorbed during compression is determined for each structure by calculating area under stress–strain curve (Equation (1)). SEA of auxetic structure is calculated by using Equation (2). Results of compressive test of auxetic structures of ABS and PLA materials are given in Table 2.

$$W = \int_0^{\varepsilon} \sigma(\varepsilon) d\varepsilon \tag{1}$$

$$\text{SEA} = \frac{W}{\Delta\rho + \rho s} \tag{2}$$

where, $\Delta\rho$ = relative density of structure, ρs = density of bulk material.

3 | RESULTS AND DISCUSSION

Table 3 gives means and SD of responses with respect to process parameters.

3.1 | Influence of process parameters on responses

ANOVA is performed to determine significance of process parameters on responses. Table 4 gives main, interaction, and quadratic influence of process parameters on

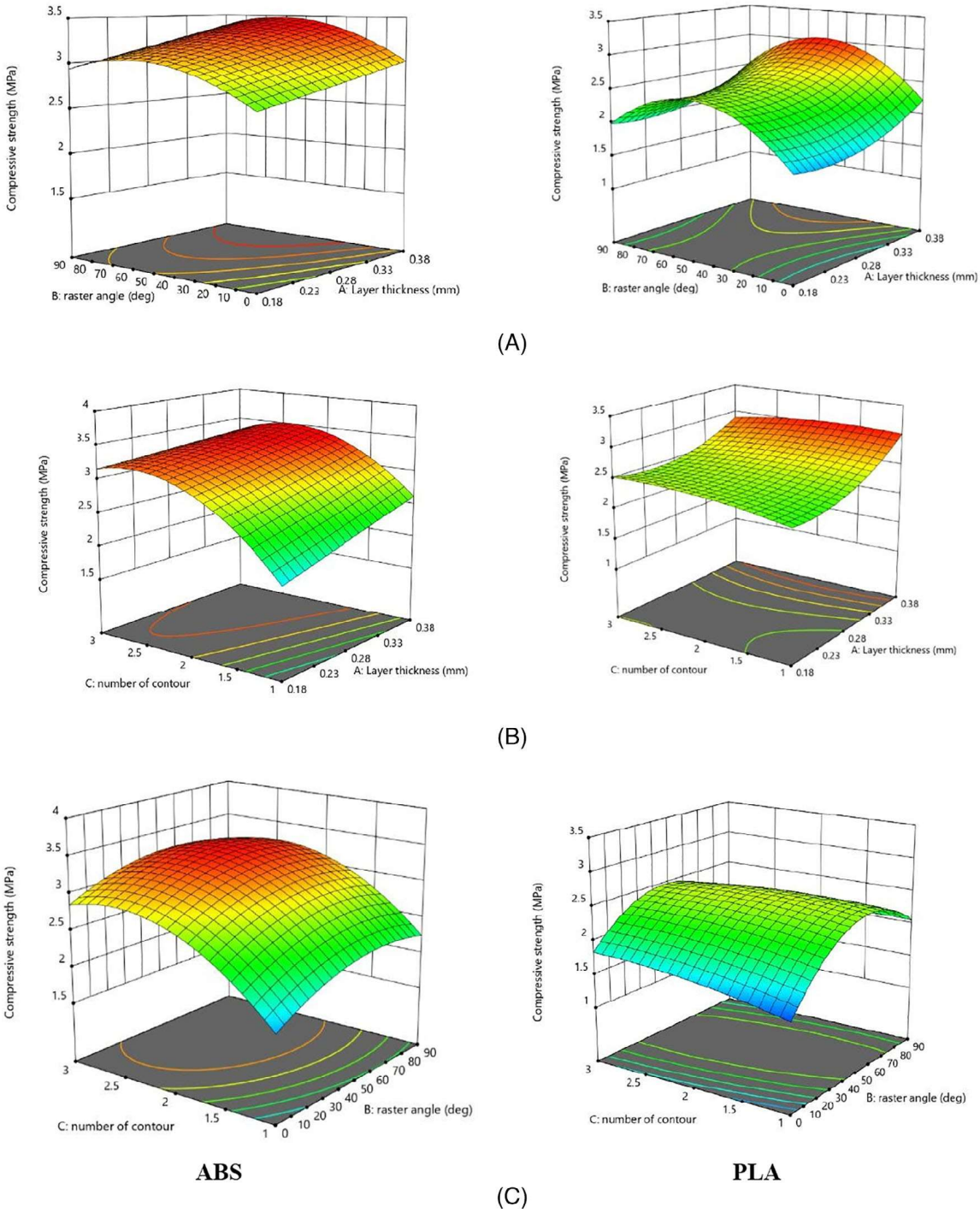

FIGURE 3 Effect of process parameters on compressive strength. A, raster angle and layer thickness; B, raster angle and layer thickness; and C, number of contour and raster angle. ABS, acrylonitrile butadiene styrene; PLA, poly-lactic acid [Color figure can be viewed at wileyonlinelibrary.com]

responses. Figure 3 depicts the effect of process parameters on compressive strength of ABS structures and PLA structures. The effects of process parameters on compressive stiffness and SEA are shown in Figures 4 and 5, respectively.

From Table 4, it is observed that layer thickness and raster angle are most influential parameters for compressive strength of auxetic structures of both materials. As depicted in Figure 3, variation of compressive strength is directly proportional to the layer thickness of structure. As layer thickness increases, number of layers required for building the structure decreases; thus, number of interlayer bond also decreases. It results in minimization of warping between successive layers due to temperature variation and thus compressive strength of structure increases. Compressive strength initially increases and

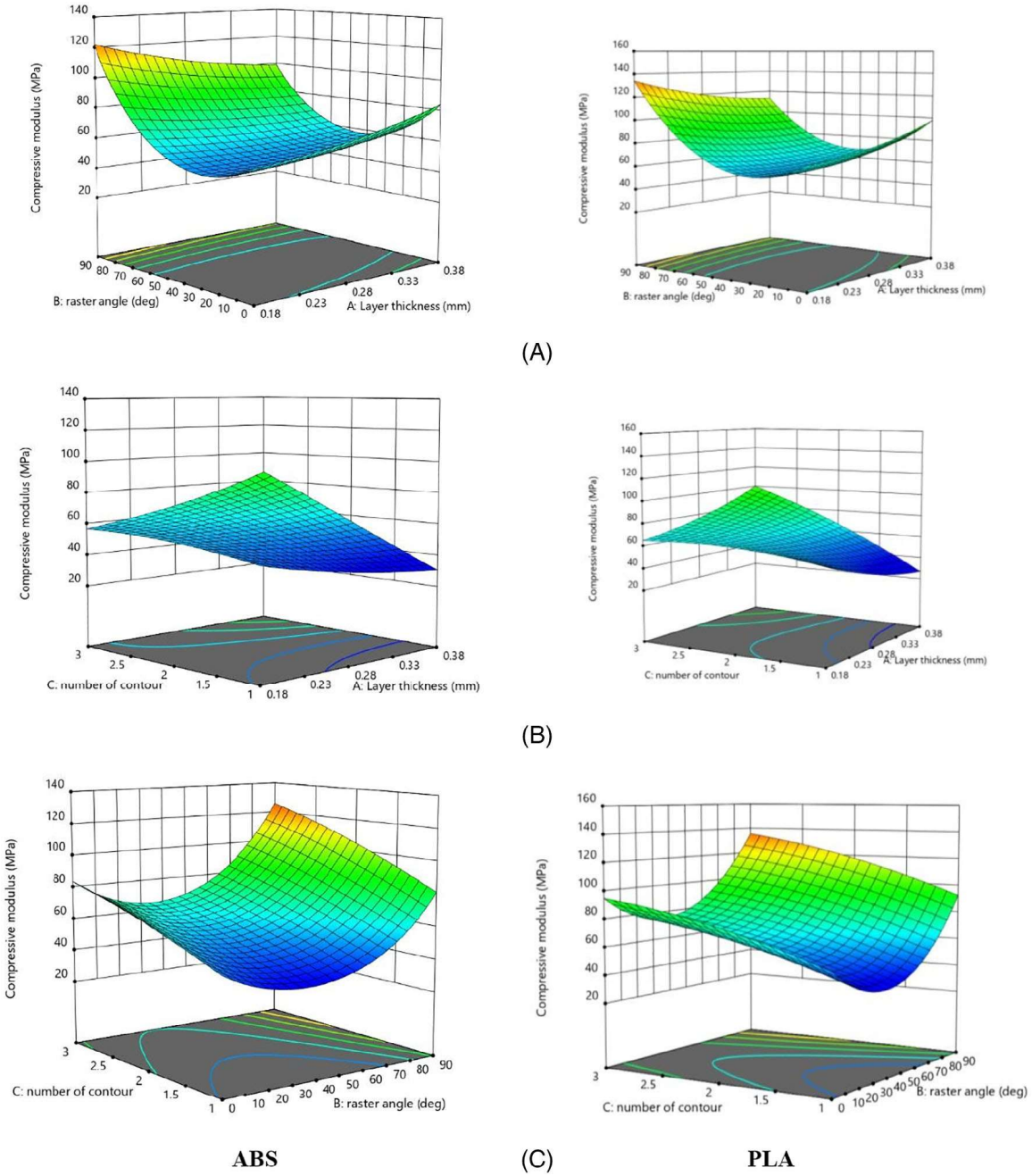

FIGURE 4 Effect of process parameters on compressive stiffness. A, raster angle and layer thickness; B, number of contour and layer thickness; and C, number of contour and raster angle. ABS, acrylonitrile butadiene styrene; PLA, poly-lactic acid [Color figure can be viewed at wileyonlinelibrary.com]

then decreases with increase in raster angle. For zero to 45° raster angle, not enough resistance is offered by rasters to the movement of platen because of sliding between them. This resistance is maximum at raster angle of around 45° due to sandwich effect of raster in between layers which results in maximum strength. As raster angle increases from 45° to 90°, this resistance reduces due to sliding effect which results in decrease in compressive strength.

For compressive stiffness of structures of both materials, raster angle and number of contours are found most significant parameters. As shown in Figure 4, compressive stiffness initially decreases and then increases with increase in raster angle. Stiffness is the resistance offered by the structure against deformation on applying load. With increase in raster angle from zero to 45°, deformation in between adjacent rasters increases which results in decrease in stiffness. Stiffness is minimum at 45° raster angle due to minimum deformation. As raster angle increases from 45° to 90°, deformation starts reducing which result in increase in stiffness. Compressive stiffness increases with increases in number of contours. As

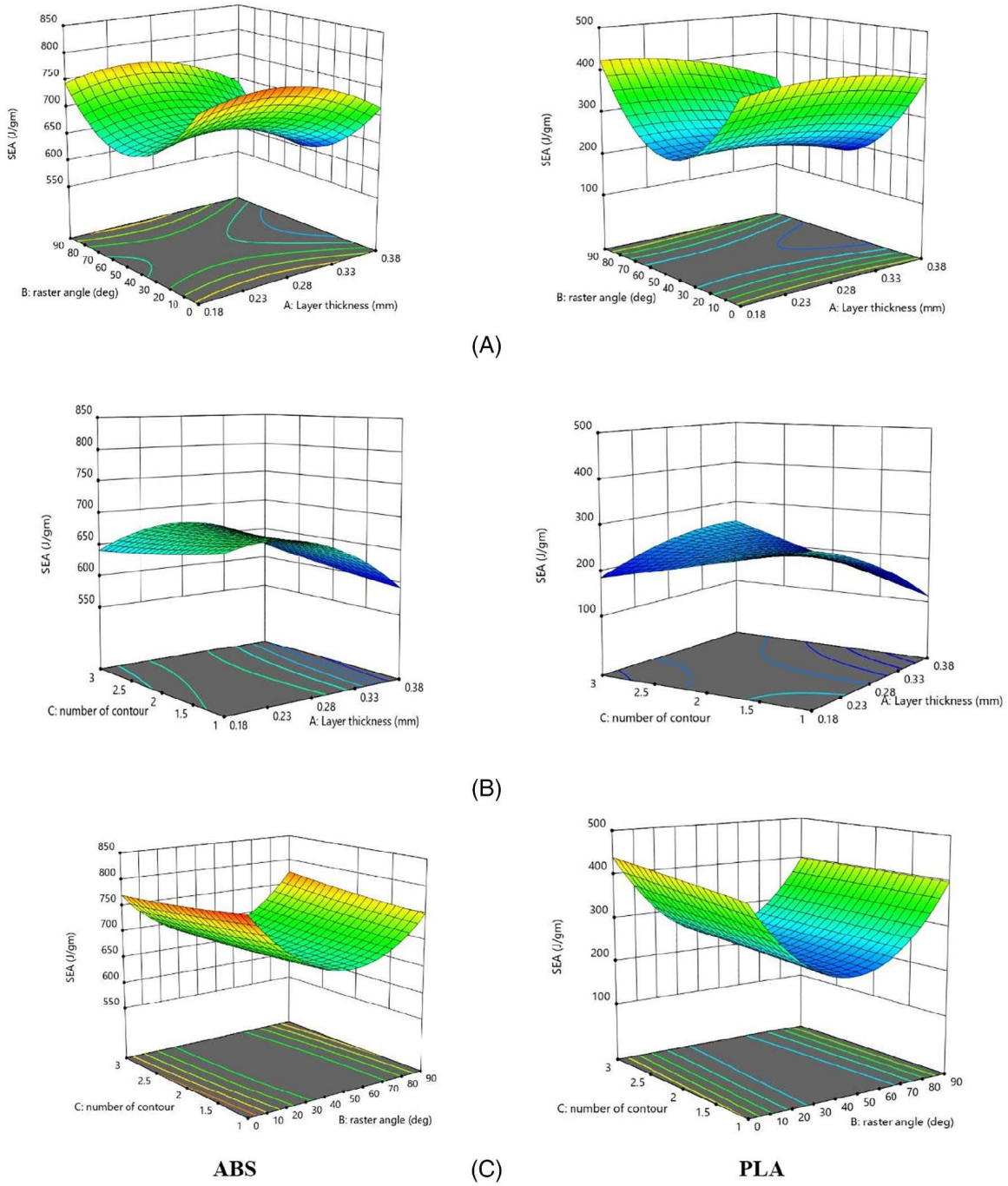

FIGURE 5 Effect of process parameters on SEA. A, raster angle and layer thickness; B, number of contour and layer thickness; and C, number of contour and raster angle. SEA, specific energy absorption [Color figure can be viewed at wileyonlinelibrary.com]

number of contours increases, zone of stress concentration shifts towards center of the structure. Specimen normally fails by shearing at stress concentration zone.[26] Therefore, moving of stress concentration region toward the center reduces chances of failure at edge resulting in increased stiffness.[9] Also, there is no requirement of rasters, when walls of the structure are filled by contours. It results in minimum cavities in fabricated structures and thus high stiffness.

For SEA of ABS structures, layer thickness and raster angle are the most influential parameters. For PLA structures it is found that SEA is influenced mainly by layer thickness. As shown in Figure 5, SEA of auxetic structures of both materials increases with decrease in layer thickness. With decrease in layer thickness, number of layers (obviously number of interlayer bonds) to fabricate structure increases. As more energy is required to break these increased number of interlayer bonds, therefore

TABLE 5 Regression models for strength, stiffness and SEA of auxetic structures

Material	ABS	PLA
Compressive strength (MPa)	$(-1.23) + (4 \times A) + (0.02 \times B) + (2.72 \times C) + (0.008 \times A \times B) - (1.07 \times A \times C) - (0.0002 \times B \times C) + (0.06 \times A^2) - (0.0001 \times B^2) - (0.5 \times C^2) - (0.003 \times A \times B \times C)$	$(1.63) - (8.49 \times A) + (0.04 \times B) + (0.73 \times C) + (0.006 \times A \times B) - (0.79 \times A \times C) - (0.002 \times B \times C) + (22.82 \times A^2) - (0.0003 \times B^2) - (0.08 \times C^2) - (0.003 \times A \times B \times C)$
Compressive stiffness (MPa)	$((9.28) - (19.2 \times A) - (0.03 \times B) - (0.3 \times C) - (0.14 \times A \times B) + (8 \times A \times C) + (0.0003 \times B \times C) + (18.43 \times A^2) + (0.0009 \times B^2) - (0.2 \times C^2))^2$	$(103.51) - (422.12 \times A) - (0.34 \times B) - (1.72 \times C) - (3.32 \times A \times B) + (146.27 \times A \times C) - (0.077 \times B \times C) + (465.23 \times A^2) + (0.018 \times B^2) - (4.94 \times C^2) + (0.36 \times A \times B \times C)$
SEA (J/g)	$(658.8) + (1717.4 \times A) - (5.2 \times B) - (71.1 \times C) - (0.1 \times A \times B) + (164.5 \times A \times C) + (0.2 \times B \times C) - (4087.95 \times A^2) + (0.049 \times B^2) + (2.96 \times C^2)$	$(562.5) - (30.56 \times A) - (6.47 \times B) - (148.89 \times C) - (4.57 \times A \times B) + (604.34 \times A \times C) - (0.2 \times B \times C) - (2203.98 \times A^2) + (0.09 \times B^2) - (0.45 \times C^2)$

Abbreviations: A, layer thickness (mm); ABS, acrylonitrile butadiene styrene; B, raster angle (degree); C, number of contours; PLA, polylactic acid; SEA, specific energy absorption.

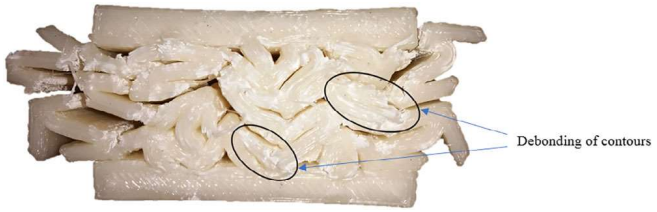

FIGURE 6 Compression tested auxetic structure showing debonding of contours [Color figure can be viewed at wileyonlinelibrary.com]

SEA of structure increases. Also, SEA of ABS structures initially decreases and then increases with increase in raster angle. At 45° raster angle, there is deformation between adjacent rasters, which offers minimum resistance to movement of platen and thus minimum SEA.[38] As PLA is a brittle material, therefore no such deformation of adjacent rasters is observed in structures. Based on ANOVA, regression models of compressive strength, stiffness, and SEA of auxetic structures of ABS and PLA materials are generated by using the Design-Expert 11 software. All regression models are given in Table 5. It is found that model predictions are in good agreement with experimental results.

3.2 | Microstructural characterization

The fracture zones of the auxetic structures are studied using SEM to examine the probable microscopic details for the failure. The SEM images give a good perception about the layer interface, voids, and non-uniformities in fabricated structure at microscopic level. Figure 6 shows compression tested auxetic structure highlighting debonding of contours. Figure 7 depicts SEM images of fractured specimens of both materials.

Defects such as porosity (ie, voids), non-homogeneous raster distribution, and weak interlayer bonding (due to shrinkage, molecular diffusion, and cross-linking between layers) are observed in SEM images. This weak interlayer bonding gives path for crack-propagation as shown in Figure 7. The main reason of these defects is uneven temperature distribution of rasters causes distortion and interlayer porosity; during fabrication. Voids/pores get enlarged on applying compressive load on the auxetic structure, and thus stress concentration in these regions increases which results in lesser strength and stiffness as compared to specimen manufactured by injection molding, multi jet modeling and ballistic particle manufacturing.[40,41] Anisotropic properties of FDM fabricated structures are also responsible for less strength.[42] Also, the interfacial de-bonding between rasters and layers occurs on applying compressive load on the auxetic structure. It influences the overall stress-strain behavior of the structure. As interfacial bonding between raster breaks, the load carrying capacity in that region decreases. But rasters still carry load in bonded region. This uneven bonding creates regions of high stress concentration, which results in bending followed by fracture of rasters. It is observed from the SEM images of failed structures that de-bonding at interface between rasters, and fracture of the raster are the main reasons of failure of auxetic structure.

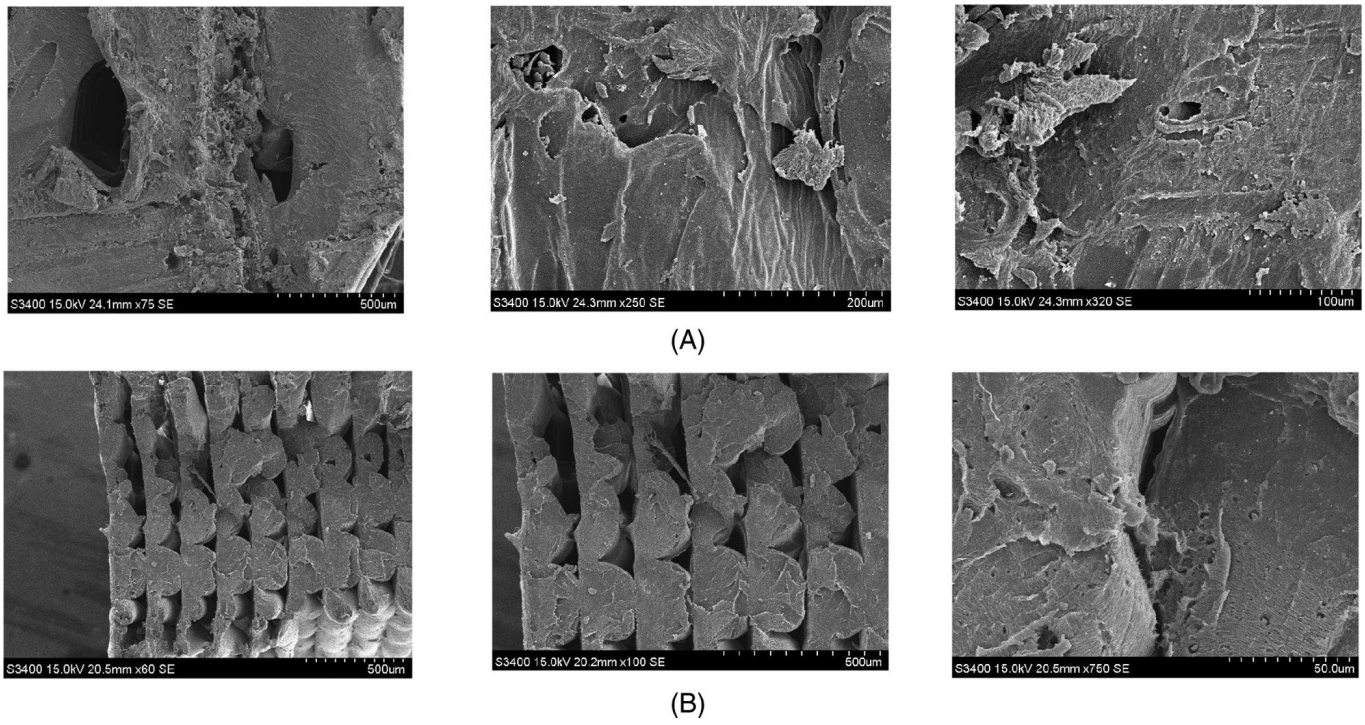

FIGURE 7 SEM images of sample fractured auxetic structures showing. A, voids; B, nonhomogeneous raster distribution, and weak interlayer bonding. SEM, scanning electron microscope

TABLE 6 Criteria for optimization and optimized values of responses

Material		ABS				PLA		
Sr. No.	Factors and responses	Goal	Lower bound	Upper bound	Optimized value	Lower bound	Upper bound	Optimized value
1	Layer thickness (mm)	In range	0.18	0.38	0.289	0.18	0.38	0.38
2	Raster angle (degree)	In range	0	90	90	0	90	0
3	Number of contours	In range	1	3	2.89	1	3	3
4	Compressive strength (N/mm^2)	Maximize	1.54	3.4	3.16	1.35	3.07	2.26
5	Compressive stiffness (N/mm^2)	Maximize	36.74	134.73	124.44	38.84	148.1	127.42
6	SEA (J/g)	Maximize	598.78	801.2	772.61	192.74	490.47	470.89

Abbreviations: ABS, acrylonitrile butadiene styrene; PLA, poly-lactic acid; SEA, specific energy absorption.

As layer thickness increases number of layers required to build the structure decreases. This results in lesser distortion because of low temperature gradient between top and bottom layer of the structure. It causes increase in compressive strength and stiffness of auxetic structures. However, as layer thickness decreases number of layers required to build the structure increases. This result in increase in SEA of the structure as energy applied during compressive loading is used in breaking more number of interlayer bonds. With change in raster angle failure mechanism of rasters varies. With raster angle of about 45°, rasters offer more resistance to the applied load, which results in increased strength and decreased stiffness and SEA. As number of contours increases, walls of the auxetic structure are filled by contours itself and there is no requirement of rasters as shown in Figure 6. Thus, voids in the walls are reduced which result in improved strength and stiffness but reduced SEA of the structure.

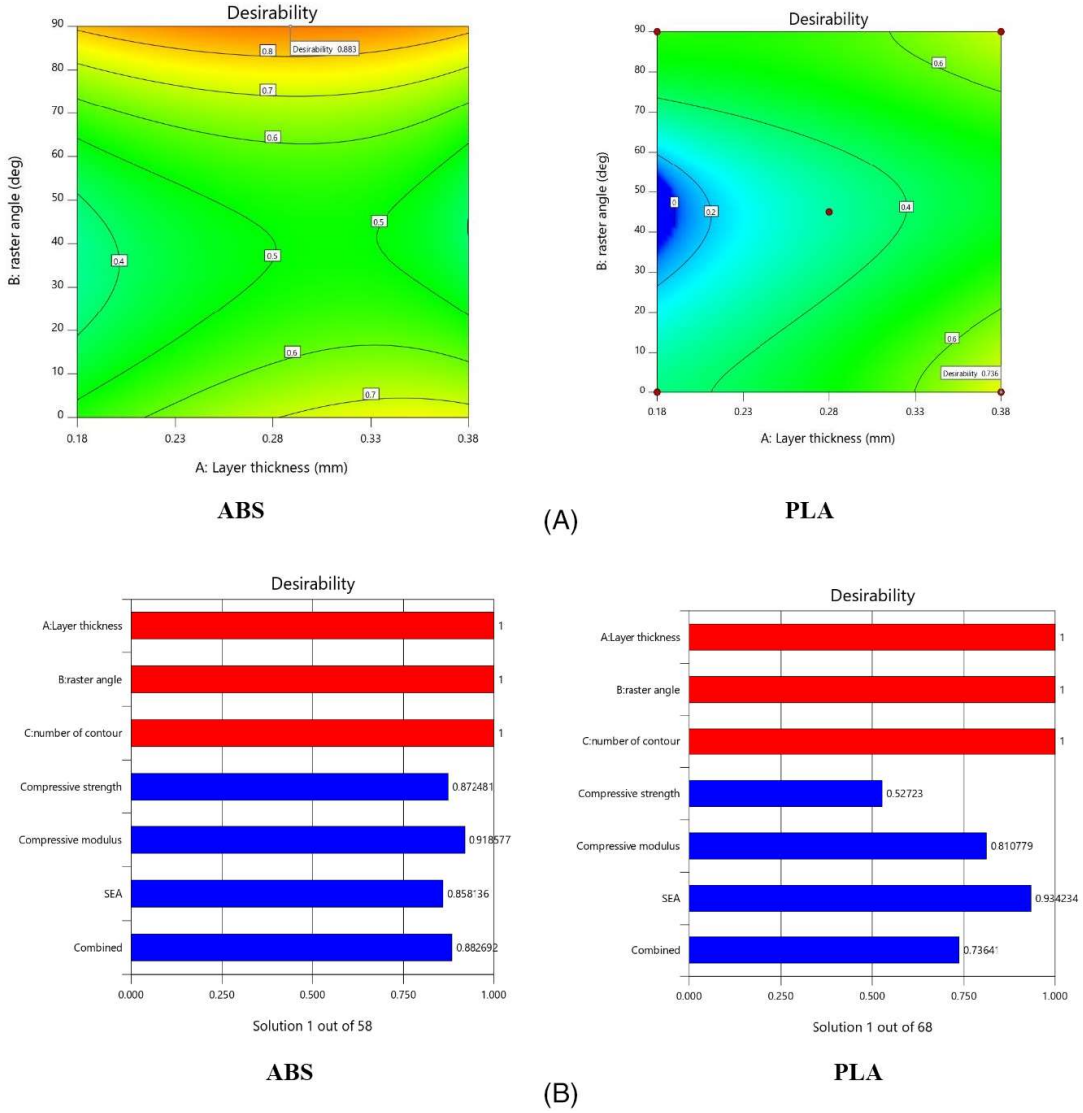

FIGURE 8 A, Desirability value with optimum levels and B, Bar graph of desirability [Color figure can be viewed at wileyonlinelibrary.com]

3.3 | Optimization of process parameters

The optimum combination of process parameters is determined to maximize compressive strength, stiffness, and SEA with the help of desirability analysis technique. Responses are related with each other in an unitless entity that is, desirability function which is constrained between 0 and 1; where 0 and 1 are undesirable and desirable response, respectively. The desirability of each response is calculated as reported in literature.[43,44] Optimized values of layer thickness, raster angle and number of contours are obtained which simultaneously fulfills optimization criteria for each response. Table 6 gives criteria for optimization and optimized values of compressive strength, compressive stiffness, and SEA for ABS and PLA structures. Figure 8 shows desirability values with optimum levels and bar graph of desirability of ABS and PLA structures. Desirability values of all responses are close to one and therefore agreeable.

3.4 | Confirmation tests

Random and optimized levels of parameters are selected and confirmation experiments are performed.[45] Confirmation tests results for random values and optimum setting of factors are given in Tables 7 and 8, respectively. Deviation percentage is calculated using Equation 3, which is less than 10%, therefore acceptable.

$$\text{deviation}\% = \frac{|\text{Predicted value} - \text{Observed value}|}{\text{Predicted value}} \times 100\% \quad (3)$$

TABLE 7 Confirmation tests results for random levels of process parameters

Material	Experiment no.	Factors			Compressive strength (MPa)			Compressive stiffness (MPa)			SEA (J/g)		
		Layer thickness	Raster angle	Number of contour	Predicted	Observed	Deviation, %	Predicted	Observed	Deviation, %	Predicted	Observed	Deviation, %
ABS	1	0.20	15	2	2.87	2.73	5.14	54.54	52.35	4.18	712.9	765.8	6.91
	2	0.30	30	1	2.27	2.39	5.03	34.45	37.24	7.50	680.5	723.4	5.93
PLA	1	0.20	15	2	2.10	2.32	9.57	61.83	64.79	4.57	313.3	337.8	7.25
	2	0.30	30	1	2.37	2.62	9.58	32.99	34.58	4.59	224.8	229.7	2.14

Abbreviations: ABS, acrylonitrile butadiene styrene; PLA, poly-lactic acid; SEA, specific energy absorption.

TABLE 8 Confirmation tests results for optimized levels of process parameters

Material	ABS									PLA								
	Compressive strength (MPa)			Compressive stiffness (MPa)			SEA (J/g)			Compressive strength (MPa)			Compressive stiffness (MPa)			SEA (J/g)		
Experiment no.	Predicted	Observed	Deviation, %	Predicted	Observed	Deviation, %	Predicted	Observed	Deviation, %	Predicted	Observed	Deviation, %	Predicted	Observed	Deviation, %	Predicted	Observed	Deviation, %
1	3.16	3.02	4.62	124.44	113.73	8.61	772.61	723.98	6.3	2.26	2.09	7.54	127.42	118.78	6.78	470.89	441.79	6.18
2	3.16	2.9	8.41	124.44	128.98	3.65	772.61	718.45	7.01	2.26	2.46	8.91	127.42	139.98	9.85	470.89	498.15	5.79
3	3.16	3.48	9.99	124.44	115.73	7.00	772.61	821.79	6.37	2.26	2.13	5.72	127.42	120.79	5.21	470.89	509.24	8.14
Average deviation, %			7.67			6.42			6.56			7.39			7.28			6.70

Abbreviations: ABS, acrylonitrile butadiene styrene; PLA, poly-lactic acid; SEA, specific energy absorption.

The fracture zones of the auxetic structures are studied using SEM [model: 3400 N Hitachi]. Samples are coated with carbon to enhance conductivity. Study is performed to examine the probable microscopic details for the failure.

4 | CONCLUSION

In this article, research work focused on experimental study of compressive strength, stiffness, and SEA of reentrant auxetic structures of ABS and PLA materials fabricated by FDM is described. It is found that layer thickness and raster angle are most influential control factors for compressive strength of auxetic structures. Compressive strength improves with increase in layer thickness. But with increase in raster angle, it increases first and then decreases. Compressive stiffness of auxetic structures is influenced mainly by raster angle and number of contours. It initially decreases and then increases with increase in raster angle, while it increases with increase in number of contours. For SEA of auxetic structures, layer thickness is most significant parameter. It increases with decrease in layer thickness. Defects, such as porosity (ie, voids), nonhomogeneous raster distribution, and weak interlayer bonding, are observed in SEM images of fractured auxetic structures.

Based on the analysis of experimental results, regression models are developed to predict compressive strength, stiffness, and SEA of auxetic structures. Also, optimization of process parameters is performed to optimize compressive strength, stiffness, and SEA. From confirmation experiments, good agreement is found between regression models and experimental results.

The present study is certainly useful in setting of process parameters to maximizing strength, stiffness, and SEA of auxetic structures fabricated by FDM. Future work will be focused on investigating strength, stiffness, and SEA of auxetic structures under shear and flexural loading.

CONFLICT OF INTEREST

The authors declare no potential conflicts of interest.

ORCID

Swapnil Vyavahare https://orcid.org/0000-0001-6133-2437

REFERENCES

[1] X. Yu, J. Zhou, H. Liang, Z. Jiang, L. Wu, *Prog. Mater. Sci.* **2018**, *1*(94), 114.
[2] J. Elipe, A. Lantada, *Smart Mater. Struct.* **2012**, *21*(10), 105004.
[3] X. Zhang, D. Yang, *Materials* **2016**, *9*(11), 900.
[4] I. Durgun, *Rapid Prototyp. J.* **2015**, *21*, 412.
[5] M. Meier, K. Tan, M. Lim, L. Chung, *Business Process Management J.* **2019**, *25*, 456.
[6] R. García-García, M. González-Palacios, *Int. J. Adv. Manuf. Technol.* **2018**, *98*(1–4), 645.
[7] N. Ahmed, P. Xue, *Int. J. Mech. Sci.* **2019**, *161*, 105062.
[8] T. Li, L. Wang, *Compos. Struct.* **2017**, *1*(175), 46.
[9] F. Scarpa, S. Blain, T. Lew, D. Perrott, M. Ruzzene, J. Yates, *Composites, Part A* **2007**, *38*(2), 280.
[10] T. Wang, L. Wang, Z. Ma, G. Hulbert, *Mater. Des.* **2018**, *160*, 284.
[11] H. Sarvestani, A. Akbarzadeh, H. Niknam, K. Hermenean, *Compos. Struct.* **2018**, *15*(200), 886.
[12] H. Sarvestani, A. Akbarzadeh, A. Mirbolghasemi, K. Hermenean, *Mater. Des.* **2018**, *15*(160), 179.
[13] A. Alomarah, D. Ruan, S. Masood, I. Sbarski, B. Faisal, *Int. J. Adv. Manuf. Technol.* **2018**, *96*(5–8), 2013.
[14] C. Lam, X. Mo, S. Teoh, D. Hutmacher, *Mater. Sci. Eng., C* **2002**, *20*(1–2), 49.
[15] E. Negis, In US-TURKEY Workshop On Rapid Technologies, **2009**, *24*, 23–30.
[16] J. Korpela, A. Kokkari, H. Korhonen, M. Malin, T. Närhi, J. Seppälä, *J. Biomed. Mater. Res., Part B* **2013**, *101*(4), 610.
[17] T. Okwuosa, D. Stefaniak, B. Arafat, A. Isreb, K. Wan, M. A. Alhnan, *Pharm. Res.* **2016**, *33*(11), 2704.
[18] M. Bayar, Z. Aziz, *J. Arch. Eng.* **2018**, *24*(3), 05018003.
[19] C. Bellehumeur, M. Bisaria, J. Vlachopoulos, *Polym. Eng. Sci.* **1996**, *36*(17), 2198. https://doi.org/10.1002/pen.10617.
[20] K. Ang, K. Leong, C. Chua, M. Chandrasekaran, *Rapid Prototyp. J.* **2006**, *12*, 100.
[21] G. Dong, G. Wijaya, Y. Tang, Y. Zhao, *Addit. Manuf.* **2018**, *2018*(19), 62.
[22] H. Dave, S. Rajpurohit, N. Patadiya, S. Dave, K. Sharma, S. Thambad, V. Srinivasn, K. Sheth, *Int. J. Mod. Manuf. Technol.* **2019**, *11*(1), 21.
[23] L. Magalhães, N. Volpato, M. Luersen, *J. Braz. Soc. Mech. Sci. Eng.* **2014**, *36*(3), 449.
[24] J. Rossiter, A. Johnson, G. Bingham, *3D Print. Addit. Manuf.* **2020**, *7*(1), 19.
[25] G. Ye, H. Bi, L. Chen, Y. Hu, *3D Print. Addit. Manuf.* **2019**, *6*(6), 333.
[26] S. Ahn, M. Montero, D. Odell, S. Roundy, P. Wright, *Rapid Prototyp. J.* **2002**, *8*, 248.
[27] A. Bellini, S. Güçeri, *Rapid Prototyp. J.* **2003**, *9*, 252.
[28] A. Sood, R. Ohdar, S. Mahapatra, *Mater. Des.* **2010**, *31*(1), 287.
[29] S. Vyavahare, S. Teraiya, D. Panghal, S. Kumar, *Rapid Prototyp. J.* **2020**, *26*, 176.
[30] E. Cuan-Urquizo, E. Barocio, V. Tejada-Ortigoza, R. Pipes, C. Rodriguez, A. Roman-Flores, *Materials* **2019**, *12*(6), 895.
[31] A. Dey, N. Yodo, *J. Manuf. Mater. Process.* **2019**, *3*(3), 64.
[32] M. Too, K. Leong, C. Chua, Z. Du, S. Yang, C. Cheah, S. Ho, *Int. J. Adv. Manuf. Technol.* **2002**, *19*(3), 217.
[33] H. Vanaei, M. Shirinbayan, M. Deligant, K. Raissi, J. Fitoussi, S. Khelladi, A. Tcharkhtchi, *Polym. Eng. Sci.* **2020**, *60*, 1. https://doi.org/10.1002/pen.25419.
[34] S. Hosseini, A. Khodakarami, E. Nxumalo, *Polym. Eng. Sci.* **2020**, *60*, 1. https://doi.org/10.1002/pen.25417.
[35] H. Kolken, A. Zadpoor, *RSC Adv.* **2017**, *7*(9), 5111.
[36] A. Ingrole, A. Hao, R. Liang, *Mater. Des.* **2017**, *117*, 72.

[37] I. Gibson, D. Rosen, B. Stucker, *Additive manufacturing technologies*, Vol. 17, Springer, New York **2014**.
[38] J. Xu, Y. Wu, L. Wang, J. Li, Y. Yang, Y. Tian, Z. Gong, P. Zhang, S. Nutt, S. Yin, *Mater. Des.* **2018**, *156*, 446.
[39] S. Raeisi, P. Tapkir, F. Ansari, A. Tovar, *SAE Tech. Pap*, SAE International, Warrendale, Pennsylvania **2019**.
[40] M. Uddin, M. Sidek, M. Faizal, R. Ghomashchi, A. Pramanik, *J. Manuf. Sci. Eng.* **2017**, *139*(8), 081018-1.
[41] J. Kotlinski, *Rapid Prototyp. J.* **2014**, *20*, 499.
[42] A. Sood, R. Ohdar, S. Mahapatra, *J. Adv. Res.* **2012**, *3*(1), 81.
[43] A. Khuri, *Response surface methodology and related topics*, World scientific, New Jersey, **2006**.
[44] S. Aksezer, *J. Ind. Manage. Optimization*. **2008**, *4*, 685.
[45] W. Jensen, *J. Qual. Technol.* **2016**, *48*(2), 162.

How to cite this article: Vyavahare S, Kumar S. Re-entrant auxetic structures fabricated by fused deposition modeling: An experimental study of influence of process parameters under compressive loading. *Polym Eng Sci*. 2020;1–14. https://doi.org/10.1002/pen.25546